

The effects of intense magnetic fields on Landau levels in a neutron star

Z. F. Gao^{1,2,3} • N. Wang¹ • J. P. Yuan¹ • Chih-Kang. Chou⁴

Abstract In this paper, an approximate method of calculating the Fermi energy of electrons ($E_F(e)$) in a high-intensity magnetic field, based on the analysis of the distribution of a neutron star magnetic field, has been proposed. In the interior of a Neutron star, different forms of intense magnetic field could exist simultaneously and a high electron Fermi energy could be generated by the release of magnetic field energy. The calculation results show that: $E_F(e)$ is related to density ρ , the mean electron number per baryon Y_e and magnetic field strength B .

Keywords Magnetar. Landau levels. Ultrastrong magnetic fields. Neutron star. Fermi energy

1 Introduction

The surface of a neutron star(NS) is widely thought to have magnetic strengths as high as 10^{13} G. The inner magnetic field is assumed to be higher than that at the surface, and may be confined within the crust

Z. F. Gao

¹Xinjiang Astronomical Observatory, CAS, 40-5 South Beijing Road, Urumqi Xinjiang, 830011, China zhifu_gao@uao.ac.cn

²Graduate University of the Chinese Academy of Sciences, 19A Yuquan Road, Beijing, 100049, China

³Department of Astronomy, Nanjing University, Nanjing, 210093, China

N. Wang

Xinjiang Astronomical Observatory, CAS, 40-5 South Beijing Road, Urumqi Xinjiang, 830011, China

J. P. Yuan

Xinjiang Astronomical Observatory, CAS, 40-5 South Beijing Road, Urumqi Xinjiang, 830011, China

Chih-Kang. Chou

National Astronomical Observatories, Chinese Academy of Sciences, Beijing, 100012, China

or may be distributed throughout the entire neutron star. Thompson and Duncan (1996) predicted that higher magnetic fields could exist in the interiors of these so-called magnetars, which are strongly magnetized neutron stars with field strengths several orders of magnitude greater than in common radio pulsars. Soft-gamma repeaters (SGRs) or anomalous X-ray pulsars (AXPs) are considered as candidates for magnetars (Colpi et al. 2000), although this assumption requires further confirmation (Harding et al. 1999).

For an ideal gas in equilibrium, the distribution function $f(E)$ can be expressed as

$$f(E) = \frac{1}{\exp[(E - \mu)/kT] \pm 1}, \quad (1)$$

where the upper sign refers to fermions (Fermi-Dirac statistics), the lower sign to bosons (Bose-Einstein statistics); k and μ represent Boltzmann's constant and the particle chemical potential (also called the Fermi energy E_F), respectively. For a completely degenerate fermion gas ($T \rightarrow 0$, i.e., $\mu/kT \rightarrow \infty$), when $E \leq E_F$, $f(E) = 1$; when $E > E_F$, $f(E) = 0$. For a massive cooling neutron star, it is the pressure associated with degenerate matter at zero temperature that supports the entire star against gravitational collapse. If all electrostatic interactions are ignored, the electron gas could be treated as ideal (noninteracting) at $T = 0$. $E_F(e)$ then has the simple form

$$E_F(e) = [p_F^2(e)c^2 + m_e^2c^4]^{\frac{1}{2}}, \quad (2)$$

with $p_F(e)$ the electron Fermi momentum. In the interior of a NS, when B is too weak to be taken into consideration, $p_F(e)$ is mainly determined by matter density (hereafter referred to as ρ) and the mean electron number per baryon (hereafter referred to as Y_e) (Shapiro & Teukolsky 1983). The influence of a high magnetic field on the equilibrium composition of

a NS has been shown in detail in previous studies (Yakovlev et al. 2001; Lai & Shapiro 1991). On the basis of the distribution characteristics of Landau levels, we introduce an approximate method for calculating the electron Fermi energy, which holds in two different systems: an ideal neutron-proton-electron (hereafter abbreviated to npe) gas and the more realistic system of Baym, Pethick and Sutherland (hereafter abbreviated to BPS) (Baym et al. 1971) consisting of a Coulomb lattice of heavy nuclei embedded in an electron gas (in the crust), where the electron Fermi energy is very small $\sim(1-25)$ MeV corresponding to $\rho \sim (10^4 - 10^{11})$ erg cm $^{-3}$ (Beskin et al. 1993). Our method additionally holds in two different magnetic fields: a weakly quantizing field and a non-quantizing field.

This paper is organized as follows: in § 2, we summarize NS structure and NS magnetic field, and consider the influences of magnetic fields on NS matter and some simple non-equilibrium processes; in § 3, we deduce an equation involving $E_F(e)$, ρ , B and Y_e , which is suitable for ultrastrong magnetic fields; in § 4, a dispute on $E_F(e)$ in intense magnetic fields is presented. A brief conclusion is given in § 5.

2 Effects of magnetic fields on neutron star matter

This section is divided into three parts. To aid interpretation of later sections, we review briefly the distribution of a NS magnetic field and the relationship between the neutron star magnetic field and Landau levels. The details are as follows.

2.1 Structure of a neutron star

A NS can be subdivided into an atmosphere and four main internal regions (the outer crust, the inner crust, the outer core, and the inner core), where the electron Fermi energy grows with ρ .

The atmosphere is a thin layer of plasma which determines the spectrum of thermal electromagnetic radiation of the star. The geometrical depth of the atmosphere varies from some ten centimeters in a hot star down to some millimeters in a cold one. The outer crust, consisting of nuclei and electrons, extends from the bottom of the atmosphere to the layer of density $\rho_d \approx 4 \times 10^{11}$ g cm $^{-3}$, at which the Fermi energy $E_F(n) = E_F(e) = 25$ MeV, and has a depth of a few hundred meters (Shapiro & Teukolsky 1983). Owing to its relatively low density, it contains about 10^{-5} of the total star mass. At $\rho \leq 10^4$ g cm $^{-3}$, the electron

gas may be non-degenerate and the ionization may be incomplete; for $\rho < 10^7$ g cm $^{-3}$, the ground state is $^{56}_{26}\text{Fe}$, the nuclei capture electrons and become neutron-rich at density $\sim 10^9$ g cm $^{-1}$; and the neutrons start to drip from the nuclei and form a free neutron gas at $\rho = \rho_d$. The inner crust, composed mainly of degenerate relativistic electrons and non-relativistic nuclei over-saturated with neutrons, extends from density ρ_d at the upper boundary to $\sim 0.5\rho_0$ at the base, and can be several kilometers deep, where $\rho_0 = 2.8 \times 10^{14}$ g cm $^{-3}$ is the standard nuclear density. When at the crust-core interface $\sim 1.4 \times 10^{14}$ g cm $^{-3}$, the nuclei disappear completely.

The outer core, consisting of neutrons mixed with a small number of protons and electrons, occupies the density range $0.5\rho_0 \leq \rho \leq 2\rho_0$ and has a depth of several kilometers. When density approaches ρ_0 , there are so many neutrons that about ninety-five percent of particles are neutrons, with only a small fraction of protons and electrons ($Y_e = Y_p \sim 0.05$) (Becker et al. 2009; Tsuruta et al. 2002). For $\rho \gg \rho_0$, where the electron Fermi energy $E_F(e) > m_\mu c^2 = 105.7$ MeV, a small fraction of muons (μ) appear (Yakovlev et al. 2001). It is worthwhile to note that a three-component liquid (neutrons, protons and electrons) is in equilibrium under mutual β -transformations. The inner core is about several kilometers in radius and has a central density as high as $\sim 10\rho_0$. For the inner core of a NS, with still further increase of density it becomes energetically more economic if some nucleons transform to ‘exotic’ particles such as hyperons, pion condensates, kaon condensates and quarks, etc, when $\rho > \rho_{tr}$, ρ_{tr} is the transition density to these ‘exotic’ particles, which is $\sim 4\rho_0$ (Becker et al. 2009; Tsuruta et al. 2002; Tsuruta et al. 2009). The maximum of the inner core density could exceed this transition density, so hyperons, pion condensates, kaon condensates, quarks and nucleons with large Y_e are expected in the inner core of a NS (Tsuruta et al. 2002; Tsuruta et al. 2009).

2.2 Magnetic fields of a neutron star

Different forms of strong magnetic field could exist in the interior of a magnetar at the same time. For instance, in the absence of superconductivity, the magnetic field is uniform on microscopic scales, and many Landau levels are occupied by the particles participating in neutrino reactions because the Fermi energies of the particles are too high. For example, protons and electrons occupy ~ 300 Landau levels in a non-quantizing strong magnetic field $\sim 10^{16}$ G at a density of about $1 \sim$ several ρ_0 (Yakovlev et al. 2001). The neutrino emissivities in such cases are about the same

as in the non-magnetized matter because the effects of magnetic quantization on the neutrino emissivities are usually too weak.

On the contrary, if in the regions where protons are superconducting and neutrons are superfluid, the magnetic field most likely exists in the form of the quantized magnetic flux tubes (fluxoids), in such case, the majority of the electrons are restricted to the ground Landau level by this field referred to as strongly quantizing magnetic field; in addition to these two types, an important phenomenon under study is called weakly quantizing, which often occurs at low temperatures and high densities, when only a few Landau levels are populated.

If the superhigh magnetic fields of magnetars originate from the induced magnetic fields by the ferromagnetic moments of the 3P_2 Cooper pairs of the anisotropic neutron superfluid at a moderate lower temperature ($T \ll 2.87 \times 10^8$ K, the critical temperature of the 3P_2 neutron superfluid) and high nuclear density ($\sim 0.5\rho_0 < \rho < 2.0\rho_0$), then the maximum of magnetic field strength for the heaviest magnetar may be estimated to be 3.0×10^{15} G according to our model (Peng & Tong 2007, 2009).

2.3 Influences of magnetic fields on star matter

The magnetic field greatly influences the properties of the NS matter. In particular, for the crust of a NS, when in a strong magnetic field $B \sim 10^{12}$ G, individual atoms will be elongated in the direction of this external field (Flower et al. 1977; Flower & Itoh 1979). In this case, crystals consisting of such atoms differ substantially from normal crystals, so there must clearly be anisotropy in their properties. The influence of the magnetic field on the crust matter structure of a NS is determined by the parameter η (Ruderman 1971). The expression for η is

$$\eta = a_0/Za_B \simeq 15B_{12}^{1/2}Z^{-3/2}, \quad (3)$$

where a_0 , Z , a_B and B_{12} are the first Bohr radius of hydrogen atom, nuclear charge number, the radius of the electron cloud in the quantizing magnetic field and the magnetic field in units of 10^{12} G, respectively (Ruderman 1971); a_B can be expressed as $a_B = (\hbar/m\omega_B)^{1/2}$ (Landau & Lifshitz 1965). The external magnetic field determines the shell structure of external electrons if $\eta \gg Z^{-3/2}$.

A superhigh field ($B \geq B_{cr}$) can strongly quantize particle motion, modify the phase space of protons (electrons), shift the beta-equilibrium, increase the proton (electrons) fraction (Chakrabarty et al. 1997; Lai & Shapiro 1991), change the nuclear shell energies and nuclear magic numbers, and therefore influence the

nuclear composition and the equation of states of the inner crust of a NS. Furthermore, magnetic fields $\sim 10^{20}$ G may cause a substantial $n \rightarrow p$ conversion, and as a result the system, composed of an ideal neutron-proton-electron gas, may be converted to highly proton-rich matter (Chakrabarty et al. 1997). However, magnetic fields of such magnitude inside NSs are uncertain and are also unauthentic. To date, there have been no observations indicating the existence of fields $B \geq 10^{16}$ G, in a NS interior; moreover, according to the virial theorem, a magnetic field $B \geq 10^{18}$ G cannot exist in a NS because the magnetic field energy ($\sim R^3B^2/6$) would predominate over the gravitational binding energy ($\sim 3GM^2/5R$), such that a dynamical instability in the hydrostatic configuration would be induced by this ultrastrong magnetic field (Shapiro & Teukolsky 1983; Lai & Shapiro 1991).

3 Electron Fermi energy in superhigh magnetic fields

We now consider a uniform magnetic field B directed along the z -axis. In this case, in the Landau gauge the vector potential \vec{A} reads $\vec{A} = (-By, 0, 0)$. For extremely strong magnetic fields, the cyclotron energy becomes comparable to the electron rest-mass energy, and the transverse motion of the electron becomes relativistic. We can define a relativistic magnetic field (often called a quantum critical magnetic field B_{cr}) by the relation $\hbar\omega = m_e c^2$, which gives $B_{cr} = m_e^2 c^3 / e\hbar = 4.414 \times 10^{13}$ G. The electron energy levels may be obtained by solving the relativistic Dirac equation in a strong magnetic field with the result

$$E_e = [m_e^2 c^4 (1 + \nu \frac{2B}{B_{cr}}) + p_z^2 c^2]^{1/2} \quad (4)$$

where the quantum number ν is given by $\nu = n + \frac{1}{2} + \sigma$ for the Landau level $n = 0, 1, 2, \dots$, spin $\sigma = \pm \frac{1}{2}$ (Canuto & Ventura 1977), and the quantity p_z is the z -component of the electron momentum and may be treated as a continuous function. Combining $B_{cr} = m_e^2 c^3 / e\hbar$ with $\mu_e = e\hbar / 2m_e c$ gives

$$E_e^2 = m_e^2 c^4 + p_z^2 c^2 + (2n + 1 + \sigma) 2m_e c^2 \mu_e B, \quad (5)$$

where $\mu_e \sim 0.927 \times 10^{-20}$ ergs G $^{-1}$ is the magnetic moment of an electron. According to the Pauli exclusion principle, the electrons are situated in disparate energy states in order one by one from the lowest energy state up to the Fermi energy (the highest energy) with the highest momentum $p_F(z)$ along the magnetic field, and the electron energy state in a unit volume, N_{pha} , should be equal to the electron number density, n_e . It is

convenient to define a non-dimensional magnetic field: $B^* = B/B_{cr}$ and the electron momentum perpendicular to the magnetic field $p_\perp = m_e c \sqrt{(2n+1+\sigma)B^*}$. Using the relation $2\mu_e B_{cr}/m_e c^2 = 1$ and summing over electron energy states in a 6-dimension phase space, we can express N_{pha} as follows:

$$N_{pha} = \frac{2\pi}{h^3} \int dp_z \sum_{n=0}^{n_m(p_z, \sigma, B^*)} \sum g_n \int \delta\left(\frac{p_\perp}{m_e c} - [(2n+1+\sigma)B^*]^{\frac{1}{2}}\right) p_\perp dp_\perp, \quad (6)$$

where $\delta(\frac{p_\perp}{m_e c} - [(2n+1+\sigma)B^*]^{\frac{1}{2}})$ is the Dirac δ -function. For $n = 0$, the spin is antiparallel to B , the spin quantum number $\sigma = -1$, so the ground state Landau level is non-degenerate; whereas at higher levels $n > 0$ are doubly degenerate, and the spin quantum number $\sigma = \pm 1$. Therefore the spin degeneracy $g_n = 1$ for $n = 0$ and $g_n = 2$ for $n \geq 1$, then Eq.(5) can be rewritten

$$N_{pha} = 2\pi \left(\frac{m_e c}{h}\right)^3 \int d\left(\frac{p_z}{m_e c}\right) \left[\sum_{n=0}^{n_m(p_z, \sigma, B^*)} \int \delta\left(\frac{p_\perp}{m_e c} - (2nB^*)^{\frac{1}{2}}\right) \left(\frac{p_\perp}{m_e c}\right) d\left(\frac{p_\perp}{m_e c}\right) + \sum_{n=1}^{n_m(p_z, \sigma, B^*)} \int \delta\left(\frac{p_\perp}{m_e c} - (2(n+1)B^*)^{\frac{1}{2}}\right) \left(\frac{p_\perp}{m_e c}\right) d\left(\frac{p_\perp}{m_e c}\right) \right], \quad (7)$$

where the maximum z -momentum $p_F(z)$ is defined by

$$[p_F(z)c]^2 + m_e^2 c^4 + (2n+1+\sigma)m_e^2 c^4 B^* \equiv E_F^2(e). \quad (8)$$

The maximum Landau level number n_m is the upper limit of the summation over n in Eq.(7), which is uniquely determined by the condition $[p_F(z)c]^2 \geq 0$ (Lai & Shapiro 1991). The expression for n_m is

$$n_m(\sigma = -1) = \text{Int}\left[\frac{1}{2B^*} \left[\left(\frac{E_F(e)}{m_e c^2}\right)^2 - 1 - \left(\frac{p_z}{m_e c}\right)^2 \right]\right], \quad (9)$$

$$n_m(\sigma = 1) = \text{Int}\left[\frac{1}{2B^*} \left[\left(\frac{E_F(e)}{m_e c^2}\right)^2 - 1 - \left(\frac{p_z}{m_e c}\right)^2 \right] - 1\right], \quad (10)$$

where $\text{Int}[x]$ denotes an integer value of the argument x . Eq.(7) may now be rewritten

$$N_{pha} = 2\pi \left(\frac{m_e c}{h}\right)^3 \int_0^{\frac{E_F(e)}{m_e c^2}} \left[\sum_{n=0}^{n_m(p_z, \sigma=-1, B^*)} \sqrt{n} + \sum_{n=1}^{n_m(p_z, \sigma=1, B^*)} \sqrt{n+1} \right] \sqrt{2B^*} d\left(\frac{p_z}{m_e c}\right). \quad (11)$$

The term $\sum_{n=1}^{n_m(p_z, \sigma=1, B^*)} \sqrt{n+1}$ can be treated as

$$\sum_{n=1}^{n_m(p_z, \sigma=1, B^*)} \sqrt{n+1} = \sum_{n=0}^{n_m(p_z, \sigma=1, B^*)} \sqrt{n+1} - (\sqrt{1} + \sqrt{0}) = \sum_{n'=0}^{n'_m(p_z, \sigma=1, B^*)} \sqrt{n'} - 1, \quad (12)$$

where

$$n'_m(p_z, B^*, \sigma = 1) = n_m(p_z, B^*, \sigma = -1) = \text{Int}\left[\frac{1}{2B^*} \left[\left(\frac{E_F(e)}{m_e c^2}\right)^2 - 1 - \left(\frac{p_z}{m_e c}\right)^2 \right]\right]. \quad (13)$$

Then we have

$$N_{pha} = 2\pi \left(\frac{m_e c}{h}\right)^3 \int_0^{\frac{E_F(e)}{m_e c^2}} \sqrt{2B^*} \left[2 \sum_{n=0}^{n_m} \sqrt{n} - 1 \right] d\left(\frac{p_z}{m_e c}\right) = 4\pi \left(\frac{m_e c}{h}\right)^3 \int_0^{\frac{E_F(e)}{m_e c^2}} \sqrt{2B^*} \left[2 \sum_{n=0}^{n_m} \sqrt{n} - \frac{1}{2} \right] d\left(\frac{p_z}{m_e c}\right) = 4\pi \left(\frac{m_e c}{h}\right)^3 \sqrt{2B^*} \int_0^{\frac{E_F(e)}{m_e c^2}} \frac{2}{3} n^{\frac{3}{2}} d\left(\frac{p_z}{m_e c}\right) - 2\pi \left(\frac{m_e c}{h}\right)^3 \sqrt{2B^*} \left(\frac{E_F(e)}{m_e c^2}\right). \quad (14)$$

Note, in the crust or interior of a NS, if the density is so high that the electron longitudinal kinetic energy exceeds its rest-mass energy, or if the magnetic field is so high that the electron cyclotron energy also exceeds its rest-mass energy, the electron becomes relativistic in either case. We introduce a ratio q defined as $q = I_1/I_2$, where $I_1 = \int_0^{n_m} \sqrt{n} dn$ and $I_2 = \sum_{n=0}^{n_m} \sqrt{n}$. If we assume n_m to be 5, 6, 7, 8, 9, 10, 15, 20 and 30, then the corresponding values of q are 0.889, 0.905, 0.916, 0.925, 0.932, 0.938, 0.957, 0.967 and 0.977, respectively. It is easy to see that q increases with n_m and $q \simeq 1$ if $n \gg 1$. Therefore, when $n_m(p_z, B^*) \geq 6$, the summation formula can be approximately replaced by the following integral equation:

$$\sum_{n=0}^{n_m} \sqrt{n} \simeq \int_0^{n_m} \sqrt{n} dn = \frac{2}{3} n_m^{\frac{3}{2}}. \quad (15)$$

For simplicity, we focus on the crustal regions where the matter density is high, the magnetic field $B^* \leq 1$ (see § 2) and Eq.(15) holds approximately. Substituting

Eq.(14) into Eq.(13) we obtain

$$\begin{aligned}
N_{pha} &= 6\pi\sqrt{2B^*}\left(\frac{m_e c}{h}\right)^3 \int_0^{\frac{E_F(e)}{m_e c^2}} n_m^{\frac{3}{2}} \\
&d\left(\frac{p_z}{m_e c}\right) - 2\pi\left(\frac{m_e c}{h}\right)^3 \sqrt{2B^*}\left(\frac{E_F(e)}{m_e c^2}\right) \\
&= 6\pi\sqrt{2B^*}\left(\frac{m_e c}{h}\right)^3 \left(\frac{1}{2B^*}\right)^{\frac{3}{2}} \int_0^{\frac{E_F(e)}{m_e c^2}} \left[\left(\frac{E_F(e)}{m_e c^2}\right)^2 - 1\right. \\
&\quad \left. - \left(\frac{p_z}{m_e c}\right)^2\right]^{\frac{3}{2}} d\left(\frac{p_z}{m_e c}\right) - 2\pi\left(\frac{E_F(e)}{m_e c^2}\right)\left(\frac{m_e c}{h}\right)^3 \sqrt{2B^*} \\
&= \frac{3\pi}{B^*}\left(\frac{m_e c}{h}\right)^3 \int_0^{\frac{E_F(e)}{m_e c^2}} \left[\left(\frac{E_F(e)}{m_e c^2}\right)^2 - 1 - \left(\frac{p_z}{m_e c}\right)^2\right]^{\frac{3}{2}} \\
&d\left(\frac{p_z}{m_e c}\right) - 2\pi\left(\frac{E_F(e)}{m_e c^2}\right)\left(\frac{m_e c}{h}\right)^3 \sqrt{2B^*}. \quad (16)
\end{aligned}$$

In order to derive the formula for $E_F(e)$, we firstly introduce two non-dimensional variables χ and γ_e , which are defined as $\chi = (\frac{p_z}{m_e c})/(\frac{E_F(e)}{m_e c^2}) = p_z c/E_F(e)$ and $\gamma_e = E_F(e)/m_e c^2$, respectively, then Eq.(16) can be rewritten as

$$\begin{aligned}
N_{pha} &= \frac{3\pi}{B^*}\left(\frac{m_e c}{h}\right)^3 (\gamma_e)^4 \int_0^1 \left(1 - \frac{1}{\gamma_e^2}\right. \\
&\quad \left. - \chi^2\right)^{\frac{3}{2}} d\chi - 2\pi\gamma_e\left(\frac{m_e c}{h}\right)^3 \sqrt{2B^*}. \quad (17)
\end{aligned}$$

The electron number density is determined by

$$n_e = N_A \rho Y_e, \quad (18)$$

where $N_A = 6.02 \times 10^{23}$ is the Avogadro constant (Shapiro & Teukolsky 1983). For a given nucleus with proton number Z and nucleon number A , the relation $Y_e = Z/A$ always holds. Combining Eq.(17) with Eq.(18), we have

$$\begin{aligned}
&\frac{3\pi}{B^*}\left(\frac{m_e c}{h}\right)^3 (\gamma_e)^4 \int_0^1 \left(1 - \frac{1}{\gamma_e^2} - \chi^2\right)^{\frac{3}{2}} d\chi \\
&- 2\pi\gamma_e\left(\frac{m_e c}{h}\right)^3 \sqrt{2B^*} = N_A \rho Y_e, \quad (19)
\end{aligned}$$

where $1/\gamma_e^2$ is called the modification factor. The calculation shows that the value of $1/\gamma_e^2$ decreases with increasing $E_F(e)$, and the value of $1/\gamma_e^2$ is too small to be included in the calculation when $E_F(e) \geq 5$ MeV. Eq.(19) can be rewritten as

$$\frac{(3\pi)^2}{16B^*} (\gamma_e)^4 - 2\pi\gamma_e \sqrt{2B^*} = \left(\frac{m_e c}{h}\right)^{-3} N_A \rho Y_e, \quad (20)$$

where the relation $\int_0^1 (1 - \chi^2)^{\frac{3}{2}} d\chi = 3\pi/16$ is used. Now, we simply discuss the application conditions of Eq.(15). It is important to note that, in a non-relativistic weak field, the electron cyclotron energy is

$\hbar\omega_B = \hbar eB/(m_e c) = 11.5 B_{12}$ KeV, the maximum Landau level number $n_m \sim E_F(e)/\hbar\omega_B \sim 10^2$ or higher, where B_{12} is magnetic field in units of 10^{12} G; also, in the case of a weakly quantizing relativistic strong magnetic field ($B \sim 10^{14} \sim 10^{15}$ G), the solution of non-relativistic electron cyclotron motion equation $\hbar\omega_B$ is no longer suitable, but if this equation is used, the rest mass of an electron m_e must be replaced by its effective mass m_e^* , which is far larger than the former after taking into account the effect of relativity. In this latter case n_m could be estimated to be ~ 10 or higher, rather than 0 or 1, which shows our evaluations are reasonable. In fact, all of the analytic derivations in this Section are based on the solution of the relativistic Dirac equation for the electrons. So the range of Eq.(15) could be $B^* \sim (0.1-100)$ and $\rho \sim (10^6 \sim 10^{15})$ g cm^{-3} .

For a NS, the magnetic field varies with density, and the properties of star matter are greatly influenced by the magnetic field. Details of how magnetic fields influence the structure and the properties of a NS have been discussed briefly in §2.3. However, we can understand such influences gradually through experiments, due to the peculiar circumstances of NSs (such as ultrastrong magnetic fields and superhigh densities etc). If we take into account the influence of a strong magnetic field on a cold, neutral gas of free electrons and a single species of nucleus (Z, A), then applying the BPS system based on a semi-empirical nuclear mass formula can yield the relationship for ρ and B . The equilibrium nuclei and the maximum equilibrium densities for specific nuclei are listed in Table 1 for $B^* = 0, 0.1, 1, 10, 100$.

In Table 1, when $B \neq 0$, the nucleus transition densities become indistinguishable in the leading three digits to those that are field-free, so the transition densities no longer continue to be listed. Table 1 clearly shows that a high-intensity magnetic field alters the nucleus transition densities for the low- A nuclei. For the highest field $B = 100 B_{cr}$, ${}_{28}^{62}\text{Ni}$ is found to be absent from the equilibrium nucleus sequence. As the density increases, the nuclei become increasingly saturated with neutrons, but in all cases, neutron drip occurs at $\rho = \rho_d$. Now, for the purpose of reducing error, an approximate method for calculating $E_F(e)$ ($E_F(e) \leq 5$ MeV) is introduced. For instance, if we want to obtain the value of $E_F(e)$ corresponding to the equilibrium nucleus density $\rho = 1.34 \times 10^9$ g cm^{-3} for the nucleus ${}_{28}^{64}\text{Ni}$ when the magnetic field $B^* = 10$, we should firstly calculate the value of the integral, which is written as follows:

$$\begin{aligned}
&\int_0^1 \left(1 - \frac{1}{\gamma_e^2} - \chi^2\right)^{\frac{3}{2}} d\chi \\
&\simeq \int_0^1 \left(1 - \left(\frac{0.511}{4.31}\right)^2 - \chi^2\right)^{\frac{3}{2}} d\chi = 0.5726, \quad (21)
\end{aligned}$$

Table 1 Magnetic BPS equilibrium nuclei below neutron drip.

Name ^b	ρ_{max1}^a	ρ_{max2}^a	ρ_{max3}^a	ρ_{max4}^a	ρ_{max5}^a
	($B^* = 0$)	($B^* = 0.1$)	($B^* = 1$)	($B^* = 10$)	($B^* = 100$)
⁵⁶ Fe	7.99×10^6	8.01×10^6	9.06×10^6	4.84×10^7	4.67×10^8
⁶² Ni	2.71×10^8		2.72×10^8	3.10×10^8	1.68×10^9
⁶⁴ Ni	1.32×10^9			1.34×10^9	2.78×10^9
⁶⁶ Ni	1.54×10^9			1.52×10^9	NO ^c
⁸⁶ Kr	3.11×10^9				3.87×10^9
⁸⁴ Se	9.98×10^9				1.14×10^{10}
⁸² Ge	2.08×10^{10}				2.10×10^{10}
⁸⁰ Zn	5.91×10^{10}				5.69×10^{10}
⁷⁸ Ni	8.21×10^{10}				8.13×10^{10}
¹²⁶ Ru	1.19×10^{11}				1.20×10^{11}
¹²⁴ Mo	1.66×10^{11}				1.67×10^{11}
¹²² Zr	2.49×10^{11}				2.50×10^{11}
¹²⁰ Sr	3.67×10^{11}				
¹²² Sr	3.89×10^{11}				
¹¹⁸ Kr	4.41×10^{11}				

^aThe ‘a’ symbol indicates that ρ_{max} is the maximum density at which the nuclide is present.

^bThe ‘b’ symbol indicates that the first six nuclear masses are known experimentally. The remainder are from the Janecke-Gravey-Kelson mass formula (see (Wapstra & Bos 1976)).

^cThe ‘c’ symbol indicates that ⁶⁶Ni is found to be absent from the equilibrium nucleus sequence, so is not presented.

Note: This Table is cited from (Lai & Shapiro 1991). All the values of ρ_{max} are measured in g cm^{-3} .

where the value of $E_F(e) \sim 4.31$ MeV corresponding to $B^* = 0$ is used. Simplifying Eq.(20) gives

$$\frac{3\pi}{1} \times 0.5726(\gamma_e)^4 - 2\pi\gamma_e\sqrt{2} = \left(\frac{m_e c}{h}\right)^{-3} N_A \rho Y_e. \quad (22)$$

Inserting the values $Y_e = 0.4375$, $\rho = 1.34 \times 10^9 \text{ g cm}^{-3}$, $m_e = 9.11 \times 10^{-28} \text{ g}$, $h = 6.63 \times 10^{-27} \text{ erg s}$, $c = 3 \times 10^{10} \text{ cm s}^{-1}$ and $N_A = 6.02 \times 10^{23}$ into Eq.(22) yields $\gamma_e \sim 9.964$, then $E_F(e)$ is estimated to be $0.511 \times 9.964 \text{ MeV} \approx 5.09 \text{ MeV}$. It’s worthwhile to note that the value of $E_F(e)$ is $\sim 5.05 \text{ MeV}$ if modification factor $1/\gamma_e^2$ is ignored. From Eq.(20), it’s clear that $E_F(e)$ is a function of B , Y_e and ρ . Combining Table 1 with Table 2 can allow us to calculate $E_F(e)$ in any given intense magnetic field, the results are partly shown as follows.

In the interior of a neutron star, $E_F(e)$ is commonly determined by ρ , Y_e and B . In a given weakly quantizing strong magnetic field ($B^* \leq 1$), $E_F(e)$ increases with matter density ρ , though Y_e decreases slightly with the nucleon number A . For a perfect crystal lattice with a single nuclear species (A, Z), the magnetic field enhances the nuclear transition density, causing a significant increase of $E_F(e)$. From Table 2, we can infer that the experimental value of 0.95 MeV (see the first row of Table 2) is evidently smaller than the theoretically correct value (no less than 1 MeV) because when the electron kinetic energy is comparable to its rest energy (mc^2), the electron is relativistic. Meanwhile, the

experimental value of 2.61 MeV (see the second row of Table 2) must be higher than the theoretical value (less than 1.96 MeV), otherwise the calculated value 1.96 MeV is incorrect.

Solving Eq.(22) gives a useful special solution for $E_F(e)$

$$E_F(e) = 34.9 \left[\frac{Y_e}{0.05} \frac{\rho}{\rho_0} \frac{B}{B_{cr}} \right]^{\frac{1}{4}} \text{MeV} (B^* \geq 1). \quad (23)$$

From Eq.(23), we obtain the schematic diagrams of $E_F(e)$ vs. B and $E_F(e)$ vs. ρ as shown in Figure 1.

From Figure 1, it is clear that $E_F(e)$ increases with increasing B in the case of superhigh magnetic fields. We speculate that the high Fermi energy of electrons could be from the release of the magnetic energy according to our model.

4 A dispute on the electron Fermi energy in intense magnetic fields

This section is composed of three subsections. For each subsection we present different methods and considerations.

4.1 Interpretations of high Fermi energy of electrons

In this part, the possible interpretations of high $E_F(e)$ are given as follows.

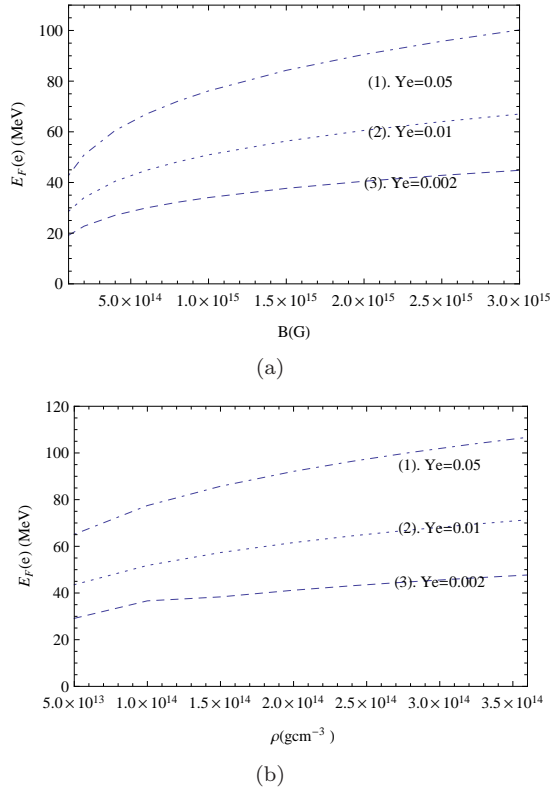


Fig. 1 Top, the electron Fermi energy dependence of the magnetic field strength when $\rho = 2.8 \times 10^{14} \text{ g cm}^{-3}$. The range of B is $(0.5 \times 10^{14} \sim 3.0 \times 10^{15}) \text{ G}$. Bottom, the electron Fermi energy dependence of the matter density when $B = 3 \times 10^{15} \text{ G}$. The range of ρ is $(0.5 \sim 3.6) \times 10^{14} \text{ g cm}^{-3}$.

Firstly, the electron Fermi energy increases with matter density. In the interior of a magnetar, magnetic fields are closely interconnected with matter density, and an extremely strong magnetic field could exist in the depths of the star where matter density $\rho \sim (10^{14} \sim 10^{15}) \text{ g cm}^{-3}$ and $E_F(e) \geq 100 \text{ MeV}$ Yakovlev et al. (2001), and the value of Y_e is expected to be higher than the mean value of Y_e of a NS, which implies that $E_F(e)$ is also expected to increase. For example, hyperon, pion condensates, kaon condensates, quarks and nucleons with large Y_e are expected in the inner core of a NS (Tsuruta et al. 2002; Tsuruta et al. 2009), the maximum of the inner core density could exceed the transition density ρ_{tr} , the value of $E_F(e)$ could be far larger than 100 MeV, accordingly.

Secondly, due to the existence of a weakly quantizing intense magnetic field and a non-quantizing intense magnetic field in the interior of a magnetar, n_{max} could be large, which implies the cyclotron energy of electrons is high, hence the electron Fermi energy is also high.

Finally, in the case of field-free (or weak field), both dp_z and dp_\perp change continuously, the microscopic state

number in a volume element of phase space $d^3x d^3p$ is $d^3x d^3p/h^3$. In the presence of an intense magnetic field, dp_z changes continuously, whereas dp_\perp is not continuous and must obey the Landau relation: $(p_\perp/m_e c)^2 = (2n + 1 + \sigma)B^*$, $n = 0, 1, 2, \dots, n_{max}(p_z, B^*, \sigma)$. For a given p_z , there is a maximum orbital quantum number $n_{max}(p_z, B^*, \sigma) \approx n_{max}(p_z, B^*)$. In superhigh magnetic fields, an envelope of these Landau cycles with maximum orbital quantum number $n_{max}(p_z, B^*)$ ($0 \leq p_z \leq p_F$) will approximately form a sphere, i.e. a Fermi sphere. The number of states in the $x-y$ plane will be less than that when the magnetic field is absent. For a given electron number density in a highly degenerate state, the stronger the magnetic field, the larger the maximum of p_z , hence the lower the number of states in the $x-y$ plane according to the Pauli exclusion principle (each microscopic state is only occupied by one electron). In other words, when B increases, both $n_{max}(p_z, B^*)$ and the number of electrons in the $x-y$ plane decrease; accordingly, the radius of the Fermi sphere p_F expands, which means that the electron Fermi energy $E_F(e)$ also increases. It should be noted that the higher the electron Fermi energy, the more obvious the ‘expansion’ of the Fermi sphere; however, the majority of the momentum space in the Fermi sphere is empty and unoccupied by electrons.

In a word, the stronger the magnetic field, the higher the electron Fermi energy; the high Fermi energy of electrons could be supplied by the release of the magnetic energy.

4.2 A wrong conclusion on the electron Fermi energy

The Fermi energy of the electrons is generally believed to decrease with the increase of the magnetic field strength for ultrastrong magnetic fields. The reasons for this are as follows: The non-relativistic Schrödinger Equation for the electrons in a uniform external magnetic field along the z -axis gives the electron energy level

$$E_e = p_z^2 c^2 / 2m_e + (2n + 1 + \sigma) \hbar \omega_B, \quad (24)$$

where $\hbar \omega_B = 2\mu_e B$, ω_B is the well-known non-relativistic electron cyclotron frequency (c.f Page 460 of Quantum Mechanics (Landau & Lifshitz 1965)). In the direction perpendicular to the magnetic field, the energy of electrons is quantized. In the interval $[p_z, p_z + dp_z]$ along the magnetic field, for a non-relativistic electron gas, the possible microstate numbers are given by

$$N_{pha}(p_z) = \frac{eB}{4\pi\hbar^2} \frac{dp_z}{c}. \quad (25)$$

Therefore, we obtain

$$N_{pha} = \int_0^{p_F} N_{pha}(p_z) dz = \frac{eB}{4\pi\hbar^2} \frac{E_F(e)}{c^2}, \quad (26)$$

where the solution of Eq.(24) is used (also c.f. Page 460 of Quantum Mechanics (Landau & Lifshitz 1965)). In the light of the Pauli exclusion principle, the electron number density should be equal to its microstate density,

$$N_{pha} = n_e = \frac{eB}{4\pi\hbar^2} \frac{E_F(e)}{c^2} = N_A \rho Y_e. \quad (27)$$

From Eq.(27), it is easy to see $E_F(e) \propto B^{-1}$ when n_e is given. We then ask why such a phenomenon exists. After careful analysis, we find that the solution of the non-relativistic electron cyclotron motion equation $\hbar\omega_B$ is incorrectly(or unsuitably) applied to calculate the energy state density in a relativistic degenerate electron gas. It's interesting to note that, in Page 12 of Canuto & Chiu (1971), in order to evaluate the degeneracy of the n -th Landau level ω_n , they first introduce the cylindrical coordinates (p_\perp, ϕ) where $\phi = \arctan p_x/p_y$, and obtain an approximate relation

$$\begin{aligned} \omega_n &= (2\pi\hbar) \int_0^{2\pi} d\phi \int_{A < p_\perp < B} p_\perp dp_\perp \\ &= 2\pi(2\pi\hbar)^{-2} \frac{(B-A)}{2} = \frac{1}{2\pi} \left(\frac{\hbar}{m_e c}\right)^{-2} \frac{B}{B_{cr}}, \end{aligned} \quad (28)$$

where $A = m^2 c^2 \frac{B}{B_{cr}} 2n$ and $B = m^2 c^2 \frac{B}{B_{cr}} 2(n+1)$ (Canuto & Chiu 1971). The authors stated clearly that this relation is valid only when $B=0$, in other words, this relation is just an approximation in the case of weak magnetic field ($B \ll B_{cr}$). Surprisingly, this relation has been misused for nearly 40 years since then. Even in some textbooks on statistical physics, the statistical weight is calculated unanimously by using the expression

$$\frac{1}{\hbar^2} \int dp_x dp_y = \frac{1}{\hbar^2} \pi p_\perp^2 \Big|_n^{n+1} = \frac{4\pi m_e \mu_e B}{\hbar^2}. \quad (29)$$

This expression will also cause the wrong deduction: $E_F(e) \propto B^{-1}$, which is exactly the same as that from Eq.(27). This wrong deduction is due to the assumption that the torus located between the n -th Landau level and the $(n+1)$ -th Landau level in momentum space is ascribed to the $(n+1)$ -th Landau level instead of using Eq.(28). Thus, the electron energy (or momentum) will change continuously in the direction perpendicular to the magnetic field, which is contradictory to the quantization of energy (or momentum) in the presence of intense magnetic field. Actually, the electrons are relativistic and degenerate in the interior of a NS, so

that Eq.(24) and Eq.(26) are no longer applicable. We therefore replace Eq.(24) and Eq.(26) by Eq.(30) and Eq.(31), respectively.

$$E_e^2 = m_e^2 c^4 + p_z^2 c^2 + (2n+1+\sigma) 2m_e c^2 \mu_e B, \quad (30)$$

$$\begin{aligned} N_{pha} &= \frac{2\pi}{h^3} \int dp_z \sum_{n=0}^{n_m(p_z, \sigma, B^*)} \sum g_n \\ &\int \delta\left(\frac{p_\perp}{m_e c} - [(2n+1+\sigma)B^*]^{\frac{1}{2}}\right) p_\perp dp_\perp, \end{aligned} \quad (31)$$

where the Dirac δ -function $\delta\left(\frac{p_\perp}{m_e c} - [(2n+1+\sigma)B^*]^{\frac{1}{2}}\right)$ must be taken into account, for otherwise we would reach the wrong conclusion that $E_F(e)$ decreases with the increase of the field strength, B , in intense magnetic fields ($B \gg B_{cr}$).

4.3 Observations of magnetars

It is widely supposed that the magnetic field is the main energy source of all the persistent and bursting emission observed in AXPs and SGRs Duncan & Thompson (1992); Mereghetti (2008). Based on the observation up to now (10 February 2011) of nine SGRs (seven confirmed) and twelve AXPs (nine confirmed) at hand, a statistical investigation of relevant parameters is possible. All known magnetars are X-ray pulsars with luminosities of $L_X \sim (10^{32} \sim 10^{36}) \text{ erg s}^{-1}$, usually much higher than the rate at which the star loses its rotational energy through spin-down Rea et al (2010). In Table 3, the persistent parameters of sixteen confirmed magnetars are listed in the light of observations performed in the last two decades.

From Table 3, we obtain the schematic diagram of magnetar's soft X-ray luminosity as a function of magnetic field strength as shown in Figure 2(a). From Figure 2(a), it's obvious that magnetar's soft X-ray luminosity increases with the increasing magnetic field strength. Furthermore, we also obtain the schematic diagrams of magnetar's soft X-ray luminosity as a function of the electron Fermi energy. The stronger the magnetic fields, the higher the electron Fermi energy becomes. Thus, magnetar's soft X-ray luminosity increases with the increasing the electron Fermi energy as shown in Figure 2(b).

It is particularly worth noting that magnetars SGR 0501+4516, SGR 0418+5729 and SGR1833+0832 with no persistent soft X/ γ -ray fluxes observed need not be considered when fitting the curves in Figure 2. In addition, according to canonical magnetar model (Duncan & Thompson 1992, 1996; Thompson & Duncan 1996), magnetar is a massive cooling isolated neutron

Table 3 AXP/SGR persistent parameters.

Name	B^a	L_X	dE/dt^b
SGR0526-66	5.6	1.4×10^{35}	2.9×10^{33}
SGR1806-20	24	5.0×10^{36c}	6.7×10^{34}
SGR1900+14	7.0	$(0.83 \sim 1.3) \times 10^{35}$	2.6×10^{34}
SGR1627-41	2.2	2.5×10^{33}	4.3×10^{34}
SGR0501+4516	1.9	NO	1.2×10^{33}
SGR0418+5729	< 0.075	NO	$< 3.2 \times 10^{29}$
SGR1833+0832	1.8	NO	4.0×10^{32}
CXOUJ0100	3.9	7.8×10^{34}	1.4×10^{33}
1E2259+586	0.59	1.8×10^{35}	5.6×10^{31}
4U0142+61	1.3	$> 5.3 \times 10^{34}$	1.2×10^{32}
1E1841-045	7.1	2.2×10^{35}	9.9×10^{32}
1RXSJ1708	4.7	1.9×10^{35}	5.7×10^{32}
CXOJ1647 ^t	1.6	2.6×10^{34}	7.8×10^{31}
1E ^t 1547.0-5408	2.2	5.8×10^{32}	1.0×10^{35}
XTEJ ^t 1810-197	2.1	1.9×10^{32}	1.8×10^{33}
1E ^d 1048.1-5937	4.2	5.4×10^{33}	3.9×10^{33}

^aThe sign ‘a’ denotes that the surface dipolar magnetic field of a pulsar can be estimated using its spin period, P , and spin-down rate, \dot{P} , by $B \simeq 3.2 \times 10^{19} (P\dot{P})^{\frac{1}{2}}$ G, where P is in seconds and \dot{P} is in seconds/second;

^bThe sign ‘b’ indicates: A pulsar slow down with time as its rotational energy is lost via magnetic dipolar radiation, and the loss rate of a pulsar’s rotational energy is noted as dE/dt ;

^cThe sign ‘c’ denotes: from Thompson & Duncan 1996;

^tThe ‘t’ symbol indicates: transient AXP;

^dThe ‘d’ symbol indicates: dim AXP.

Note: All data are from the McGill AXP/SGR online catalog of 10 Feb. 2011 (<http://www.physics.mcgill.ca/~pulsar/magnetar/main.html>) except for L_X of SGR1806-20. The units of B , L_X and dE/dt are 10^{14} G, erg s^{-1} and erg s^{-1} , respectively.

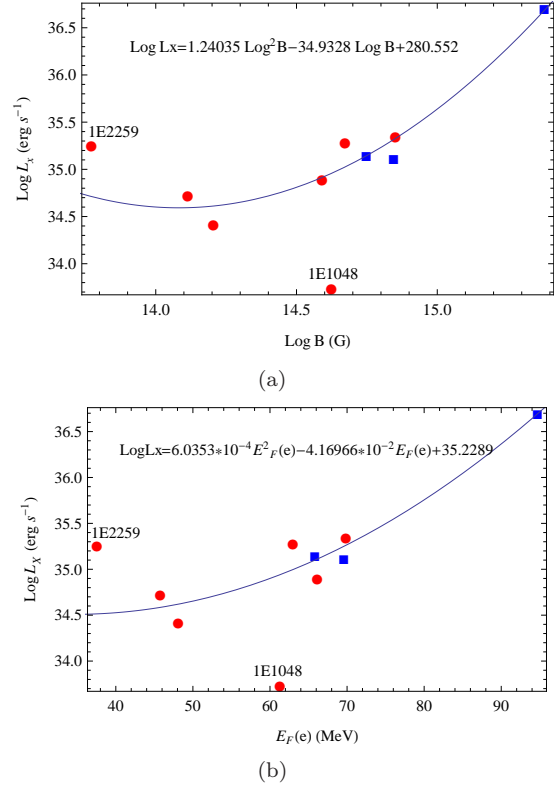


Fig. 2 Top, the fitted curve of L_X vs. B for magnetars. The range of B is $(0.5 \times 10^{14} \sim 2.5 \times 10^{15})$ G. Squares and circles mark the values of variables corresponding to SGRs and AXPs, respectively. Bottom, the fitted curve of L_X vs. $E_F(e)$ for magnetars. The range of $E_F(e)$ is $(36 \sim 96)$ MeV, where $\rho = 2.8 \times 10^{14} \text{ g cm}^{-3}$ and $Y_e = 0.05$.

star with no accretion (Yakovlev et al. 2001), and its persistent soft X-ray luminosity shouldn’t be less than its rotational energy loss rate, dE/dt , so magnetars SGR 1627-41, 1E 11547.0-5408 and XTEJ 1810-197 also should not be considered. With respect to AXPs 1E 2259+586 and 1E 1048.1-5937, their particular soft X-ray luminosities are far from the fitted curved lines, shown in Figure 2. The possible explanations are given as follows.

1. The observed properties of 1E 2259+586 seem consistent with the suggestion that it is an isolated pulsar undergoing a combination of spherical and disk accretion (White & Marshall 1984). This magnetar could be powered by accretion from the remnant of Thorne -Żytow object (TŻ (van Paradijs et al 1995)).
2. AXP 1E 1048.1-5937, discovered as a 6.4 s pulsar near the Carina Nebula Steward et al (1986), is confirmed to be a dim isolated pulsar with no mechanism to explain well its ‘abnormal’ behaviors including L_X . Observations indicated a significant decline

in variation in its persistent soft X-ray luminosity. For example, between September 2004 and February 2011, L_X decreased from $(1\sim 2) \times 10^{34}$ erg s $^{-1}$ (Mereghetti et al 2004) to 5.4×10^{33} erg s $^{-1}$.

However, in accordance with the traditional view on the electron Fermi energy, the electron capture rate Γ will also decrease with increasing B in ultrastrong magnetic fields. If the electron captures induced by field-decay are an important mechanism powering magnetar's soft X-ray emission (Cooper & Kaplan 2010), then L_X will also decrease with increasing B , which is contrary to the observed data in Table 3 and the fitting results of Figure 2.

5 Conclusions

In this paper, on the basis of the distribution of Landau levels of electrons, we derive the formulae for electron Fermi energy in ultrastrong magnetic fields. We conclude that the stronger the magnetic fields, the higher the electron Fermi energy becomes. However, the traditional viewpoint on electron Fermi energy will be confronted with a severe challenge from our calculations of $E_F(e)$. If the magnetic field is the main energy source of all the persistent and bursting emission observed in magnetars, this article could be useful in studying the direct URCA processes, neutrino emissions and neutron star cooling, etc. It is expected that that our assumptions and calculations can be used to compare with observations in the future, to provide a deeper understanding of the nature of the ultrastrong magnetic fields and soft X-ray in magnetars.

Acknowledgements We are very grateful to Prof. Qiu-He Peng, Prof. Zi-Gao Dai and Prof. Yong-Feng Huang for their help in improving our presentation. This work is supported by National Basic Research Program of China (973 Program 2009CB824800), Knowledge Innovation Program of The Chinese Academy Sciences KJCX $_2$ -YW-T09, West Light Foundation of CAS (No.280802), Xinjiang Natural Science Foundation No.2009211B35, the Key Directional Project of CAS and NSFC under projects 10173020,10673021, 10773005, 10778631,10903019 and 11003034.

Table 2 The relation of $E_F(e)$ and B .

Name	Y_e	$E_F(1)$ $B^*=0$	$E_F(2)$ $B^*=1$	$E_F(3)$ $B^*=10$	$E_F(4)$ $B^*=100$
$^{56}_{26}\text{Fe}$	0.4643	0.95 ^a	1.07 ^b	2.53 ^c	6.93 ^d
$^{62}_{28}\text{Ni}$	0.4516	2.61 ^a	1.96 ^b	3.62 ^c	9.48 ^d
$^{64}_{28}\text{Ni}$	0.4375	4.31 ^a		5.09 ^c	10.66 ^d
$^{66}_{28}\text{Ni}$	0.4242	4.45 ^a		5.17 ^c	NO ^e
$^{86}_{36}\text{Kr}$	0.4186	5.66 ^a			11.45 ^d
$^{84}_{34}\text{Se}$	0.4048	8.49 ^a			14.88 ^d
$^{82}_{32}\text{Ge}$	0.3902	11.44 ^a			17.18 ^d
$^{80}_{30}\text{Zn}$	0.3750	14.08 ^a			21.82 ^d

^aThe sign ‘a’ denotes that these values of $E_F(e)$ are known experimentally, corresponding to nuclei densities 7.96×10^6 , 2.71×10^8 , 1.30×10^9 , 1.48×10^9 , 1.48×10^9 , 1.48×10^9 , 1.10×10^{10} , 2.08×10^{10} and $5.44 \times 10^{10} \text{ g cm}^{-3}$, respectively. Each density is the maximum density at which a given nucleus survives (Hanensel & Pichon 1994);

^bThe sign ‘b’ denotes that these nuclear masses known experimentally are from the fourth column of Table 1;

^cThe sign ‘c’ denotes that these nuclear masses known experimentally are from the fifth column of Table 1;

^dThe sign ‘d’ denotes that these nuclear masses known experimentally are from the sixth column of Table 1;

^eThe sign ‘e’ denotes that $^{66}_{28}\text{Ni}$ is found to be absent from the equilibrium nucleus sequence, and so is not presented.

Note: All the values of $E_F(e)$ are measured in MeV. Despite the existence of very small mass differences caused by experimental uncertainty between the data in the second column of Table 1 and that in the third column of Table 2, the results of our calculations will not be affected. In the fourth column of Table 2, for every nucleus (from $^{64}_{28}\text{Ni}$ to $^{80}_{30}\text{Zn}$), the discrepancy between the nucleus transition density corresponding to $B^* = 1$ and the nucleus transition density corresponding to $B^* = 0$ is so small that it is almost impossible to make a significant difference. The same is true, in the fifth column of Table 2, for every nucleus (from $^{86}_{36}\text{Kr}$ to $^{80}_{30}\text{Zn}$), the discrepancy between the nucleus transition density corresponding to $B^* = 10$ and the nucleus transition density corresponding to $B^* = 0$ is also too small to be distinguished from each other, which can be seen in the fourth and the fifth column of Table 2, so the transition densities no longer continue to be listed.

References

- Beskin V. S., Gurevich A. V., Istomin Y. N., translated from the Russian by Tsaplina M.V., 1993, *Physics of the Pulsar Magnetosphere*, Cambridge University Press
- Balberg S., Barnea N., 1998, *Phys. Rev. C*, 57, 409
- Baym G., Pethick R., Sutherland P., 1971, *Astrophys. J.*, 171, 299(BPS)
- Becker W.(Editor), 2009, 'Neutron Stars and Pulsars ', *Astrophysics and Space Science Library*, 357
- Canuto V., Chiu H. Y., 1971, *Space Sci. Rev.*, 12, 3c
- Canuto V., Ventura J.,1977, *Fund. Cosmic Phys.*, 2, 203
- Chakrabarty S., Bandyopadhyay D., Pal S., 1997, *Phys. Rev. Lett.*, 78, 75
- Cooper R. L., Kaplan D. L., 2010, *Astrophys. J. Lett.*, 708, L80
- Duncan R. C., Thompson C., 1992, *Astrophys. J.*, 392, L9
- Duncan R. C., Thompson C., In: Rothschild R.E., Lingefelner R.E. (eds.) *High-Velocity Neutron Stars and Gamma-Ray Bursts*. AIP Conference Proc., vol. 366, p. 111. AIP Press, New York (1996)
- Colpi M., Geppert U., Page D., 2000, *Astrophys. J. Lett.*, 529, L29
- Flower E., Lee J. F., Ruderman M.A., et al., 1977, *Astron. J.*, 215, 291-301
- Flower E., Itoh N., 1979, *Astrophys. J.*, 230, 847
- Haensel P., Pichon B., 1994, *Astron. Astrophys.*, 283, 313
- Harding A.K., Contopoulos I., Kazanas D., 1999, *Astrophys. J. Lett.*, 525, 125
- Israel G. L., Mereghetti S., Stella L., 1994, *Astrophys. J.*, 433,L25
- Kondratyev V. N., 2002, *Phys. Rev. Lett.*, 88, 221
- Lai D., Shapiro S. L., 1991, *Astrophys. J.*, 383, 745-751
- Landau L. D., Lifshitz E. M., 1965, *Quantum mechanics*, Pergamon, Oxford
- Mereghetti S., Tiengo A., Stella L., et al.,2004,*Astrophys. J.*, 608, 427
- Mereghetti S., 2008, arXiv:0804.0250
- Paczynski B., 1992, *Acta Astron.*, 42, 145
- Peng Q.-H., Tong H., 2007, *Mon. Not. R. Astron. Soc.*, 378, 159
- Peng Qiu He., Tong Hao., arXiv:0911.2066v1 [astro-ph.HE] 11 Nov 2009, 10th Symposium on Nuclei in the Cosmos, 27 July-1 August 2008 Mackinac Island, Michigan,USA
- Pethick C. J., 1992, *Rev. Mod. Phys.*, 6(4), 1133
- Rea N., Esposito P., Turolla R., et al., 2010, *Science*, DOI 10.1126/science.1196088, arXiv:2010.2781v1
- Ruderman M. A.,1971, *Phys. Rev. Lett.*, 27,1306-1308
- Sawyer R. F., 1972, *Phys. Rev. Lett.*, 29, 382
- Shapiro S. L., Teukolsky S. A., 1983, 'Black holes,white drarfs,and neutron stars' John Wiley & Sons, New York
- Steward F., Charles P. A., Smale A. P.,1986, *Astrophys. J.*, 305, 814
- Thompson C., Duncan R. C., 1996,*Astrophys. J.*, 473, 322
- Tsuruta S.,Teter M. A., Takatsuka T., et al., 2002, *Astrophys. J. Lett.*, 571, 143
- Tsuruta S., Sadino J., Takatsuka A., et al., 2009, *Astrophys. J.*, 691, 621-632
- van Paradijs J., Taam R.E., van den Heuvel E. P. J., 1995, *Astron. Astrophys.*, 299, 41
- Wapstra A. H., Bos K., 1976, *Atomic Data Nucl. Data Tables*, 17, 474
- White N. E., Marshall F. E., 1984, *Astrophys. J.*, 281, 354
- Yakovlev D. G., Kaminker A. D., Gnedin O. Y., et al., 2001, *Phys. Rep.*, 354, 1